

D. Kuzman · S. Svetina · R. E. Waugh · B. Žekš

## Elastic properties of the red blood cell membrane that determine echinocyte deformability

Received: 6 February 2003 / Accepted: 14 June 2003 / Published online: 12 September 2003  
© EBSA 2003

**Abstract** The natural biconcave shape of red blood cells (RBC) may be altered by injury or environmental conditions into a spiculated form (echinocyte). An analysis is presented of the effect of such a transformation on the resistance of RBC to entry into capillary sized cylindrical tubes. The analysis accounts for the elasticity of the membrane skeleton in dilation and shear, and the local and nonlocal resistance of the bilayer to bending, the latter corresponding to different area strains in the two leaflets of the bilayer. The shape transformation is assumed to be driven by the equilibrium area difference ( $\Delta A_0$ , the difference between the equilibrium areas of the bilayer leaflets), which also affects the energy of deformation. The cell shape is approximated by a parametric model. Shape parameters, skeleton shear deformation, and the skeleton density of deformed membrane relative to the skeleton density of undeformed membrane are obtained by minimization of the corresponding thermodynamic potential. Experimentally,  $\Delta A_0$  is modified and the corresponding discocyte–echinocyte shape transition obtained by high-pressure aspiration into a narrow pipette, and the deformability of the resulting echinocyte is examined by whole cell aspiration into a larger pipette. We conclude that the deformability of the echinocyte can be accounted for by the mechanical behavior of the normal RBC membrane, where the equilibrium area difference  $\Delta A_0$  is modified.

**Keywords** Red blood cell deformability · Membrane elastic properties · Nonlocal bending · Echinocyte · Micropipette aspiration

### Introduction

Red blood cell (RBC) deformability, i.e., the ability of RBC to deform under applied stresses, is important for the delivery of oxygen to tissues. Important factors that determine RBC deformability include the cell volume to surface area ratio, the viscosity of the cytoplasm, and the elastic behavior of its membrane (Mohandas and Chasis 1993; Mohandas and Evans 1994).

RBC membrane consists of the phospholipid bilayer and the underlying skeleton that together determine its elastic properties. Early studies of micropipette aspiration of the RBC have already indicated the crucial role that membrane shear deformation plays in RBC deformability (Evans 1973; Evans and La Celle 1975). These analyses were performed under the assumption that the skeleton is incompressible. However, Discher et al. (1994), using fluorescence to image the deformation of the skeleton, demonstrated that the skeletal density of the pipette-aspirated membrane is non-uniform. Based on this evidence, Mohandas and Evans (1994) and Boey et al. (1998) developed elastic constitutive models of the membrane that account for the skeleton area expansivity.

The mechanical response of the phospholipid bilayer is determined by the bilayer area expansivity, and the local and nonlocal bending stiffness (Helfrich 1973; Svetina et al. 1985; Božič et al. 1992). Nonlocal bending stiffness arises from a difference between the neutral surface areas of the outer and inner bilayer leaflets ( $\Delta A$ ) that is different from its equilibrium value ( $\Delta A_0$ ). The corresponding energy is proportional to the square of the difference between the values of  $\Delta A$  and  $\Delta A_0$  (Svetina et al. 1985). The energy required to expand the bilayer area is several orders of magnitude larger than bilayer bending energy and therefore the

D. Kuzman (✉) · S. Svetina · B. Žekš  
Institute of Biophysics, Faculty of Medicine,  
University of Ljubljana, Lipičeva 2, 1000  
Ljubljana, Slovenia  
E-mail: drago.kuzman@biofiz.mf.uni-lj.si  
Tel.: +386-1-5437600  
Fax: +386-1-4315127

S. Svetina · B. Žekš  
Jožef Stefan Institute, Jamova 39, 1000 Ljubljana, Slovenia

R. E. Waugh  
Department of Pharmacology and Physiology,  
School of Medicine and Dentistry,  
University of Rochester, 601 Elmwood Ave,  
Box 711, Rochester, NY 14642-0001, USA

surface area can be considered to be constant during RBC deformation.

Several groups have observed a dependence of RBC deformability on its morphology (Meiselman 1981; Reinhart and Chien 1986; Chabanel et al. 1987; Bazzoni and Rasia 1998). The rheological behavior of crenated (echinocytes) and cupped (stomatocytes) RBCs obtained by amphipathic agents has been tested using a counter-rotating rheoscope (Meiselman 1981), microscopic photometric monolayer technique (Li et al. 1999), and by micropipette aspiration (Bessis et al. 1973; Chabanel et al. 1987). Results indicate that echinocytic as well as stomatocytic shape alterations lead to decreased cellular deformability. Li et al. (1999) clearly demonstrated that echinocyte deformability correlates with the severity of crenation, rather than with the concentration of the amphipathic agent salicylamide. On the basis of these observations it can be concluded that the bilayer also contributes to RBC deformability, because various amphipathic agents are known to exert their effect on RBC by an intercalation into its bilayer leaflets (Deuticke 1968; Sheetz and Singer 1974). The question is in what way the intercalation of amphipathic agents into the bilayer affects the mechanical stiffness of the cell as a whole. In this work it is proposed that to first order the amphipathic agents simply change the minimum energy state from which the cell must start to deform. Thus it has a longer hill to climb to get to where it is going. In this sense it is our aim to identify the mechanical properties of the membrane bilayer that have to be taken into consideration in addition to the mechanical properties of the membrane skeleton in order to interpret the apparent mechanical stiffness of the cell.

The specific objective of the presented study is to show that by including contributions from the membrane bilayer in the elastic energy of deformation (in addition to the contributions of the membrane skeleton) we can account for the behavior exhibited by echinocytes of different degrees of severity being aspirated into micropipettes. We consider both area expansivity and shear of the membrane skeleton, and local and nonlocal bending of the bilayer at constant membrane surface area. These same membrane elastic properties were shown to be required for stable echinocytic shape determination (Mukhopadhyay et al. 2002). The severity of an echinocyte is directly related to the equilibrium area difference between the membrane leaflets. To test this experimentally, we modify RBC equilibrium area difference  $\Delta A_0$  by the method described by Artmann et al. (1997) to produce RBC morphology changes of different degrees, and then we examine their deformability by whole cell micropipette aspiration. The experimental results are compared with an analysis of the cell deformation as it is aspirated into the pipette, using a parametric model to describe the shape of the partially aspirated cell, and accounting for both the membrane skeletal and membrane bilayer contributions to the energy.

## Theory

We shall list consecutively the energy terms describing the elastic properties of the RBC membrane, describe the parametric model used to simulate the RBC normal and deformed shapes, calculate the contributions of different energy terms to the energy of the aspirated and outer portions of the membrane, define the equilibrium state of the partly aspirated echinocyte, and determine the strain–stress relationship and the skeleton density distribution.

### Energy terms

The model used to calculate the energy of membrane deformation includes local and nonlocal bending energies ( $W_b$  and  $W_r$ ), associated with the bilayer, and shear and area dilatation energy ( $W_\mu$  and  $W_K$ ), associated with the membrane skeleton. The membrane is assumed to have uniform properties, and the surface area is assumed to remain constant, with an area equal to the neutral surface area of the bilayer.

The energy terms of the bilayer are given by the following expressions for the local bending energy (Helfrich 1973):

$$W_b = \frac{k_c}{2} \int (c_1 + c_2 - c_0)^2 dA \quad (1)$$

where  $k_c$  is the local bending modulus,  $c_1$  and  $c_2$  are the principal curvatures of the surface, and  $c_0$  is the spontaneous curvature, and for the nonlocal bending energy, which is proportional to the square of the difference between  $\Delta A$  and  $\Delta A_0$  (Božič et al. 1992):

$$W_r = \frac{k_r}{2h^2 A_0} (\Delta A - \Delta A_0)^2 \quad (2)$$

with

$$\Delta A = h \int (c_1 + c_2) dA \quad (3)$$

where  $k_r$  is nonlocal bending modulus and  $h$  is the distance between the neutral surfaces of the two leaflets. The normalization of the  $\Delta A$  with respect to its value for a sphere that has the surface area  $A_0$  and the radius  $R_0 = (A_0/4\pi)^{1/2}$  yields a dimensionless area difference  $\Delta a$ :

$$\Delta a = \frac{\Delta A}{8\pi R_0 h}. \quad (4)$$

For convenience we shall define the local bending energy for the case that the spontaneous curvature is zero and incorporate  $c_0$  into the nonlocal bending energy. This can be done for a given  $k_r$ , by defining an effective area difference that includes also the contribution of spontaneous curvature (Svetina et al. 1985):

$$\overline{\Delta a_0} = \Delta a_0 + k_{c,c_0 A_0} \quad (5)$$

Bilayer bending energy is then a sum of the effective local and effective nonlocal bending energies:

$$W_b = \frac{k_c}{2} \int (c_1 + c_2)^2 dA \quad (6)$$

$$W_r = 8\pi k_r (\Delta a - \overline{\Delta a_0})^2. \quad (7)$$

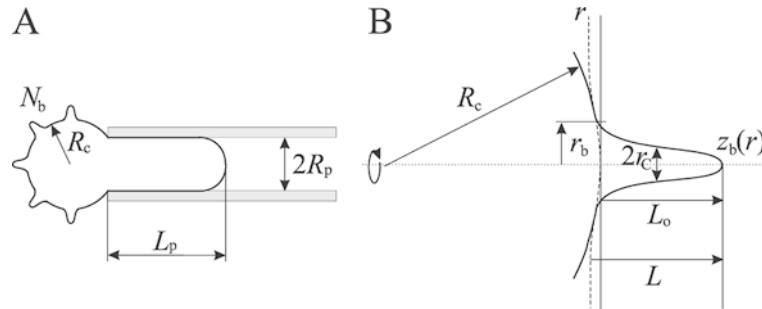
The expression for the elastic energy of the skeleton is not trivial because the elastic response is nonlinear at large deformations. To include nonlinear effects, different macroscopic (Evans and Skalak 1980; Discher et al. 1994; Eggleton and Popel 1998; Mukhopadhyay et al. 2002) and microscopic (Discher et al. 1998) descriptions of the skeleton energy have been presented in the literature. Proposed potentials differ at large deformations, while at small extensional ratios they are all proportional to the sum of invariant terms  $(\lambda_1 - \lambda_2)^2/2$  and  $(\lambda_1 + \lambda_2 - 2)^2/2$ , where the first term describes shear deformation and the second area expansivity:

$$W_\mu = \frac{\mu}{2} \cdot \int (\lambda_1 - \lambda_2)^2 dA_0 \quad (8)$$

$$W_K = \frac{K}{2} \cdot \int (\lambda_1 + \lambda_2 - 2)^2 dA_0 \quad (9)$$

with  $\mu$  the shear modulus and  $K$  the area expansivity modulus. Deformation is given in terms of the extension ratios  $\lambda_1$  and  $\lambda_2$  that describe an extension of a relaxed skeleton patch. The total surface area of the skeleton is assumed to be equal to the area of the bilayer. It is also assumed that the membrane skeleton does not contribute to the nonlocal bending of the membrane because the area expansivity modulus of the skeleton is four orders smaller than that of the bilayer (Discher et al. 1994).

**Fig. 1a, b** Shape parameterization of a partially aspirated echinocyte. **a** The cell projection is a cylinder plus a hemispherical cap with a length  $L_p$  and radius equal to the pipette radius  $R_p$ . The remaining part is a spherical cell body with radius  $R_c$  onto which a discrete number of spicules  $N_b$  are joined. **b** Enlarged scheme of a spicule with height  $L_o$  and width  $r_c$ .  $L$  is the difference between the maximum and minimum value of the contour function (Eq. 10). The radius of the spicule base is designated as  $r_b$ . The spicule contour for  $r > r_b$  and the contour of the spherical cell body covered by the spicule base are indicated with *dashed lines*, and the axis of symmetry with *dotted lines*



Elastic moduli are set to fixed values. The local bending modulus  $k_c$  of RBC membrane is set to be  $2 \times 10^{-19}$  J (Hwang and Waugh 1997) and the nonlocal bending modulus  $k_r$  is set, based on a theoretical estimate, to be  $8 \times 10^{-19}$  J. Values of the skeleton shear modulus for two-dimensional spectrin network vary from  $2.5 \times 10^{-6}$  N/m obtained from studies using optical tweezers (Lenormand et al. 2001; Hénon et al. 1999) to  $4-15 \times 10^{-6}$  N/m, obtained by RBC micropipette aspiration (Evans and La Celle 1975; Hochmuth and Waugh 1987; Discher et al. 1994). By the observation of the skeleton density of the pipette-aspirated RBC membrane the ratio between  $K$  and  $\mu$  was determined to be  $K/\mu \approx 2$  (Discher et al. 1994). Recently, Lenormand et al. (2001) measured directly the ratio  $K/\mu$  by the optical tweezers approach and they obtained  $K/\mu \approx 2-3$ . Therefore, for the present analysis we take values for  $K$  and  $\mu$  that are consistent with available data,  $\mu = 6 \times 10^{-6}$  N/m and  $K/\mu = 2$ .

### Cell shape model

The aspirated cell shape is approximated using a parametric model, where the aspirated part is assumed to be a cylinder with a hemispherical cap. The radius of the cylinder and of the cap is equal to the pipette radius  $R_p$ . The length of the aspirated part from the pipette tip to the cap apex is designated as  $L_p$ . The remaining outer cell portion is assumed to be a sphero-echinocyte and is described as a spherical cell body of a radius  $R_c$  on which a specified number of spicules, or bumps ( $N_b$ ), is distributed. At the border of a spicule and the cell body the boundary condition is set so that a spicule contour fits smoothly to the spherical cell body. The spicules are axisymmetric and their contour ( $z_b(r)$ ) is described by the following parametric function:

$$z_b(r) = \frac{L}{1 + (r/r_c)^4} \quad (10)$$

where  $r$  measures a distance from the axis of the symmetry,  $r_c$  is a characteristic spicule width,  $L$  is related geometrically to the spicule height  $L_o$  (see Fig. 1). To obtain a contour shape that resembles spicule shapes obtained by electron-microscopy (Besiss 1973), the exponent of  $r/r_c$  is taken to be four. Larger exponents (e.g., six) give rise to a spicule with a top that is too flat, whereas the exponent two results in an unrealistically

large spicule base. It should be pointed out that the energies of spicule with exponents 2, 4, and 6 differ by less than 1%. The schematic diagram of the assumed cell shape with related parameters is shown in Fig. 1.

The shape of a partly aspirated echinocyte is thus described by a set of six parameters ( $L_o$ ,  $r_b$ ,  $R_c$ ,  $r_c$ ,  $N_b$ , and  $L_p$ ). The spicule height  $L_o$ , the radius of the spicule base  $r_b$ , and the radius of the spherical cell body  $R_c$  are derived from geometrical demands that cellular volume  $V_0$  and cellular surface area  $A_0$  do not change during pipette aspiration, and that the spicule contour fits smoothly on the spherical cell body at  $r_b$ . The equations that describe these geometrical constraints are represented in Appendix A. The remaining three parameters  $r_c$ ,  $N_b$ , and  $L_p$  are obtained by minimization of thermodynamic potential at a given aspiration pressure  $\Delta P$ .

The value of the pipette radius  $R_p$  used in the model is chosen as the smallest radius that still enables complete suction of the cell with the volume  $V_0$  and surface area  $A_0$ . The magnitude of  $R_p$  is thus defined as a radius of a cylinder that is capped with two hemispheres and has the volume and surface area of the cell.  $R_p$  is determined by the following equation.

$$\frac{4}{3}\pi R_p^3 - A_0 R_p + 2V_0 = 0. \quad (11)$$

Energy contributions for aspirated and outer portions of the cell membrane

For a given shape that satisfies the geometric constraints the energy terms  $W_b$ ,  $W_r$ ,  $W_\mu$ , and  $W_K$  are calculated.  $W_b$  and  $\Delta a$  are calculated separately for the aspirated part, for the spherical cell body and for the spicule according to Eqs. (4) and (7). The total local bending energy and area difference are thus respectively equal to

$$W_b = W_b^p + W_b^s + N_b \cdot W_b^b \quad (12)$$

$$\Delta a = \Delta a^p + \Delta a^T + \Delta a^s + N_b \cdot \Delta a^b \quad (13)$$

where superscript p is assigned to the cell projection, superscript s to the spherical cell body and superscript b to the spicule (bump). All spicules are assumed to have the same shape.  $\Delta a^T$  is a leaflet area difference of a junction of the spherical cell body and the cell projection. The local bending of that junction is not taken into account because its magnitude, after the spherical cap is formed, does not vary enough to be relevant for our analysis. Detailed expressions of particular terms in Eqs. (12) and (13) are described in Appendix B.

The membrane skeleton is considered to be two dimensional and to be free to move only in lateral directions. It is assumed that the area of the relaxed skeleton is the same as the bilayer area, and that in the relaxed state, the elastic skeleton energy is equal to zero. There is conflicting evidence that the area of the relaxed skeleton may be either smaller (Boey et al. 1998) or

larger (Svoboda et al. 1992) than the bilayer area, and the simplest case is to simply take the areas to be equal. A difference between skeleton and lipid bilayer area leads to prestress of the membrane skeleton.

The initial resting shape of the membrane is assumed to be discoid (Fig. 2a). The portion of the skeleton that is aspirated into the pipette is deformed into a cylinder plus a hemispherical cap, with an axis of symmetry that matches the symmetry axis of the undeformed disk. The remaining skeleton is deformed owing to forming the outer sphero-echinocyte. The shape of the sphero-echinocyte is not symmetric and therefore treatment of the skeleton deformation due to crenation is complex. In order to simplify the study, we divide the sphero-echinocytic part of the cell into small equal axisymmetric parts, each corresponding to a

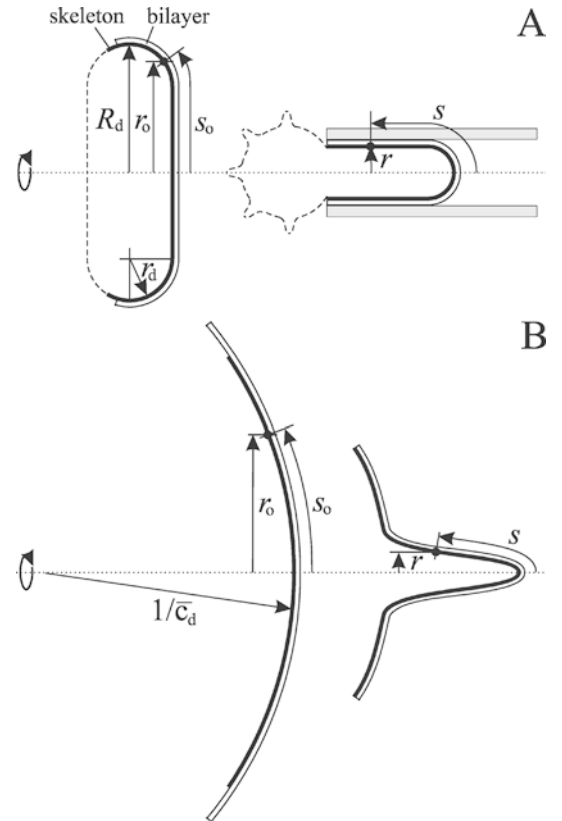


**Fig. 2a, b** Deformation of the RBC membrane skeleton. Layers corresponding to the bilayer and skeleton are indicated schematically. **A** material point is mapped from its location in the undeformed membrane (*left*) at radius  $r_0$  and surface coordinate  $s_0$ , to its location in the deformed membrane (*right*) at radius  $r$  and surface coordinate  $s$ . The axes of symmetry are shown with *dotted lines*. **a** Aspiration into the pipette. The resting cell shape is approximated as a rounded flat disk of radius  $R_d$  and thickness  $2r_d$ . The deformed section is a cylinder with a hemispherical cap. **b** Spicule formation. The resting shape of the membrane is approximated as a section of a sphere with curvature equal to the average curvature of the disk,  $\bar{c}_d$  (see Table 2, footnote). In both cases it is shown that (because of the compressibility of the skeleton) portions of the bilayer and skeleton that have equal areas in the deformed state typically have different areas in the resting state

single spicule (Fig. 2b). In reality the bases of the spicules are not axisymmetric. However, as we shall see later (Fig. 5C), the density of the skeleton in the base of the spicule does not vary appreciably. Therefore, the error resulting from this approximation should be negligible. The undeformed state is taken to be a section of a sphere with curvature equal to the mean curvature of the undeformed disk, and the deformed shape is given by Eq. (10).

Because both the resting and deformed shapes are specified, mapping of a small portion of the skeleton from its resting location, characterized by the radial coordinate  $r_0$  and the meridional coordinate  $s_0$ , to the deformed location, characterized by the radial coordinate  $r$  and the meridional coordinate  $s$ , can be accomplished with a single parametric mapping function  $s_0(s)$ , as detailed in Appendix C. (A more general approach has been taken by Mukhopadhyay et al. (2002), where the deformed shape is not specified in advance. Qualitatively similar results were obtained.) The mapping function  $s_0(s)$  is obtained by minimizing the deformation energy of the skeleton ( $W_{\text{sk}}$ ) (Eqs. 8 and 9) using calculus of variations. Deformation of a small portion of the skeleton is described by extension ratios  $\lambda_1$  and  $\lambda_2$ . For axisymmetric deformation these are defined (Evans and Skalak 1980):

$$\lambda_1 = \frac{r}{r_0} \quad \text{and} \quad \lambda_2 = \frac{d}{ds_0}. \quad (14)$$

Minimization of  $W_{\text{sk}}$  is achieved by solving the Euler–Lagrange equation. Explicit descriptions of the Euler–Lagrange equation and the initial conditions are described in Appendix C.

It is assumed that the relaxed skeleton density is uniform, and that it is modified during membrane deformation. The relative skeleton density at a point on the deformed cell is defined as follows:

$$\rho_{\text{sk}} = \frac{1}{\lambda_1 \cdot \lambda_2}. \quad (15)$$

#### Equilibrium state for a partially aspirated echinocyte

Thermodynamically, the equilibrium state of a partially aspirated erythrocyte is characterized as the minimum of the thermodynamic potential ( $G$ ) of the system. In the present model, we assume that the work done by the aspiration is entirely transformed into the elastic energy of the cell membrane. In this case, the thermodynamic potential can be defined as:

$$G = -\Delta P \cdot V_p + W_{\text{el}} \quad (16)$$

where  $V_p$  is the cell volume aspirated into the pipette and  $W_{\text{el}}$  is the membrane elastic energy:

$$W_{\text{el}} = W_\mu + W_K + W_b + W_r \quad (17)$$

where energy terms are defined by Eqs. (6), (7), (8), (9), (12) and (13). At equilibrium, the variation of the thermodynamic potential with respect to all variables is zero,  $\delta G = 0$ . The free variables of the parametric model ( $N_b$ ,  $r_c$ , and  $L_p$ ) at given  $\Delta P$  are thus derived from a set of equations:

$$\frac{\partial G}{\partial N_b} = 0, \quad \frac{\partial G}{\partial r_c} = 0, \quad \text{and} \quad \frac{\partial G}{\partial L_p} = 0. \quad (18)$$

Taking account of the expression for  $G$  given in Eq. (16), these equations can be expressed as follows:

$$\partial W \frac{\text{el}}{\partial N_b} = 0 \quad \text{and} \quad \partial W \frac{\text{el}}{\partial r_c} = 0, \quad (19)$$

$$\frac{\partial W_{\text{el}}}{\partial L_p} - \pi R_p \Delta P = 0. \quad (20)$$

In the analysis, Eqs. (19) were first solved for different fixed  $L_p$  to obtain the elastic energy as function of  $L_p$ . This function was then used to calculate the dependence of  $L_p$  on  $\Delta P$  via Eq. (20).

#### Cell response to aspiration by micropipette

RBC deformability measured by micropipette aspiration is characterized by the dependence of the equilibrium projection length on the aspiration pressure. For a certain cellular volume, cellular surface area, and given material properties, the dependence of projection length on pressure can be obtained as described above (Fig. 3). The calculated projection length increases progressively with increasing aspiration pressure. The curve becomes vertical at a critical aspiration pressure where projection length begins to increase freely at constant pressure, i.e., the cell flows into the pipette without further increases in pressure. (The dependence of projection length on pressure was not studied for  $L_p < R_p$ .)

As can be seen in Fig. 3, the relationship between projection length and aspiration pressure depends on  $\Delta a_0$ . The effect of an increase of  $\Delta a_0$  is a shift of the curve to larger values of  $\Delta P R_p$  and a decrease in the slope of the curve. The critical point also depends on  $\Delta a_0$ . Increasing  $\Delta a_0$  moves the critical point to larger values of  $\Delta P R_p$  and smaller values of  $L_p/R_p$ .

We note that aspiration of the cell into the pipette does not affect the spicule contour (Fig. 3) as much as it affects other parameters that determine the shape of sphero-echinocyte (Fig. 4). Figure 4 shows the dependence of sphero-echinocyte shape on  $\Delta a_0$ . An increase of  $\Delta a_0$  leads to a more pronounced echinocytic shape for the undeformed cell. This is manifested as an increase in the number surface density of spicules (Fig. 4d and e), a thinning of spicules (Fig. 4a), and a decrease in the proportion of the spherical cell body that is occupied by spicules (Fig. 4f).

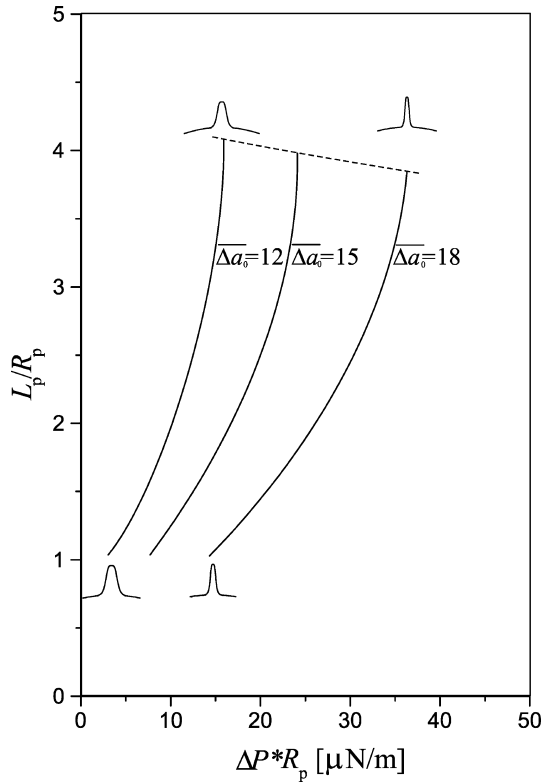


**Fig. 3** The predicted dependence of the projection length (normalized by the pipette radius) on the product of the aspiration pressure times the pipette radius for three indicated values of  $\overline{\Delta a_0}$ . Other material constants are:  $\mu = 6 \mu\text{N/m}$ ,  $K = 2\mu$ ,  $k_c = 2 \times 10^{-19} \text{ J}$ ,  $k_r = 4k_c$ ,  $V_o = 109 \mu\text{m}^3$ ,  $A_o = 140 \mu\text{m}^2$ . The pipette radius is  $1.7 \mu\text{m}$ . Critical points are connected by dashed lines. Spicule contours for  $\overline{\Delta a_0} = 12$  (left) and  $\overline{\Delta a_0} = 18$  (right) are shown at  $L_p/R_p = 1$  (below the curves) and at critical points (above the curves)

### Skeleton density distribution

An important aspect of red cell membrane behavior during deformation is that changes in membrane contour are associated with lateral redistribution of the membrane skeleton, such that the local density of the skeleton varies with position over the surface. Such changes in density can be detected by fluorescent labeling of membrane components (Discher et al. 1994). The model presented here yields a prediction for the distribution of skeletal density both in the membrane projection in the pipette and along the spicules of the echinocyte. These are shown in Fig. 5. In Fig. 5A the distribution of density along the projection length is shown for six different projection lengths. For the longest length (which corresponds to the critical pressure for cell entry into the pipette) a local density maximum occurs near the pipette entrance. This maximum begins to occur when the cell is approximately halfway into the pipette. Its location corresponds to material elements that were originally at the rim of the undeformed disk and are maximally compressed in the radial direction. For the other shorter lengths shown,

the gradients of the density along the projection length are similar, but the ratio of the density at the pipette tip to the density at the hemispherical cap decreases with decreasing projection length. The effect of changing  $\overline{\Delta a_0}$  on the skeletal density in the pipette is illustrated in Fig. 5B. As  $\overline{\Delta a_0}$  increases, larger pressures are required to form the same projection length, such that at higher  $\overline{\Delta a_0}$  the mean skeletal density in the pipette projection is shifted toward higher values of the pressure. A more subtle effect is that at the same projection length, the mean skeletal density is lower for larger values of  $\overline{\Delta a_0}$ . (Note that the curve for the largest  $\overline{\Delta a_0}$  extends the farthest below 1.0, indicating that the average density tends to be smallest when  $\overline{\Delta a_0}$  becomes large.) The distribution of skeletal density on a spicule is shown in Fig. 5C. Similar to the distribution in the pipette projection, the skeletal density is lower at the tip of the spicule and higher at its base. This tendency grows more pronounced for larger  $\overline{\Delta a_0}$  (not shown).

### Experiment

To test the predictions of the effect of echinocyte shape transformations on cell deformability, the cell shape was modified and whole cell aspiration tests were performed. A change in cell shape was induced by mechanical trauma to the cell (Artmann et al. 1997). When a discoid RBC is aspirated into a narrow pipette by high negative pressure, it takes the shape of an echinocyte when it is released. Artmann et al. (1997) postulated that this creation of the cell is driven by an increase in  $\Delta A_o$  that arises from a mechanically induced transmembrane phospholipid translocation. This shape transformation only occurs when the pipette is too small for the cell to enter easily and when large pressures are applied. Therefore, after a cell was created, tests of cell deformability were performed by aspirating the entire cell into a pipette large enough to accommodate it easily. In this case, large suction forces were not needed, and no further change in the resting cell shape was produced. Created cells relax back to their initial discoid shape with a characteristic time of approximately 15 min. The time needed to complete the whole cell deformability test was less than 1 min, such that the state of the modified cell remained essentially unchanged over the course of the measurement. However, by allowing the cells to relax between sequential tests, it was possible to measure the deformability of the same cell with multiple different initial shapes.

### Preparation of the cell suspension

Human blood was obtained from healthy volunteers. RBCs were washed three times by centrifugation and suspended at very low concentrations in hypotonic PBS (phosphate-buffered saline: 120 mmol/l NaCl,

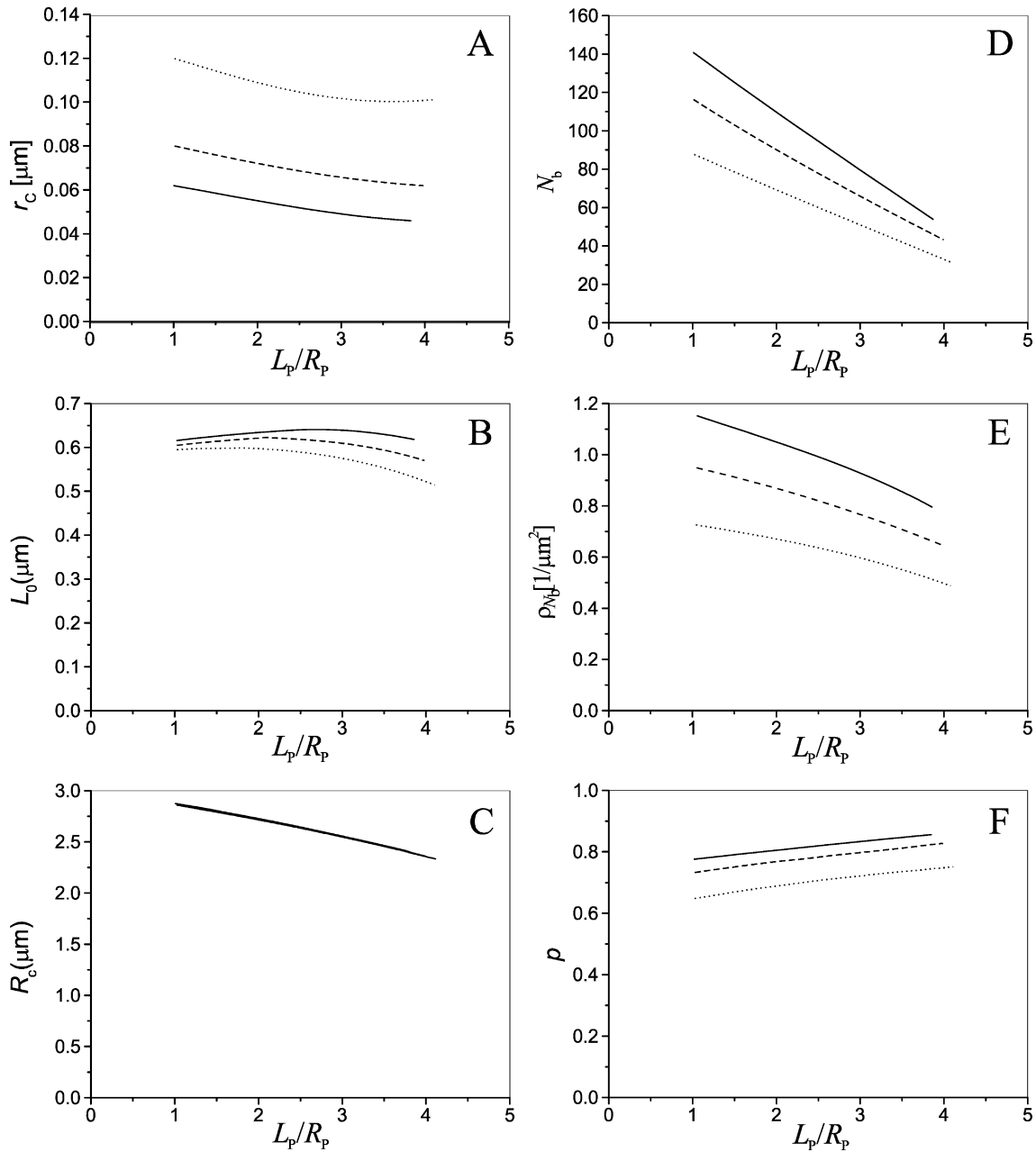


**Fig. 4a-f** Predicted dependence of geometric parameters on the projection length ( $L_p/R_p$ ) for three different values of  $\Delta a_0$  (18—solid line, 15—dashed line, and 12—dotted line). Other material constants are as in Fig. 3. **a** spicule width, **b** spicule height, **c** radius of the spherical cell body, **d** number of spicules, **e** surface density of spicules ( $N_b$  per non-aspirated RBC membrane area), and **f** fraction of the spherical cell body surface that is not taken up by spicules (i.e., the fraction of the total membrane area outside the pipette that retains its spherical contour). The point at the right end of each curve corresponds to the critical point

23.3 mmol/l  $\text{Na}_2\text{HPO}_4$ , 5.8 mmol/l  $\text{KH}_2\text{PO}_4$ , 4% fetal bovine serum (HyClone, Logan, Utah, USA), pH 7.3, 270 mOsm/kg) that was filtered through a  $0.22 \mu\text{m}$  filter. PBS was degassed by warming under vacuum for 15 min. All measurements were made at room temperature ( $22 \pm 1^\circ\text{C}$ ) within 4 h after blood collection.

## Apparatus

Micropipettes (made from Pyrex tubing, diameter  $0.9 \pm 0.05 \text{ mm}$ , wall thickness  $0.2 \pm 0.0125 \text{ mm}$ , Fredrich & Dimmock, Millville, N.Y., USA) were pulled with the aid of a pipette puller (Model 730, D. Kopf Instruments, Tujunga, Calif., USA) and broken off using a microforge to make internal tip radii of either  $0.5\text{--}0.8 \mu\text{m}$  or  $1.5\text{--}1.8 \mu\text{m}$ . The smaller pipettes were used for area and volume measurements, for high-pressure induced echinocytosis, and as pressure reference pipettes. The larger pipettes were used for whole cell aspiration. Micropipettes were filled with filtered PBS and connected to a water-filled reservoir. Pipettes were coated with 1.5% Surfasil solution (Pierce Chemical Co., Rockford, IL, USA) according to manufacturer's

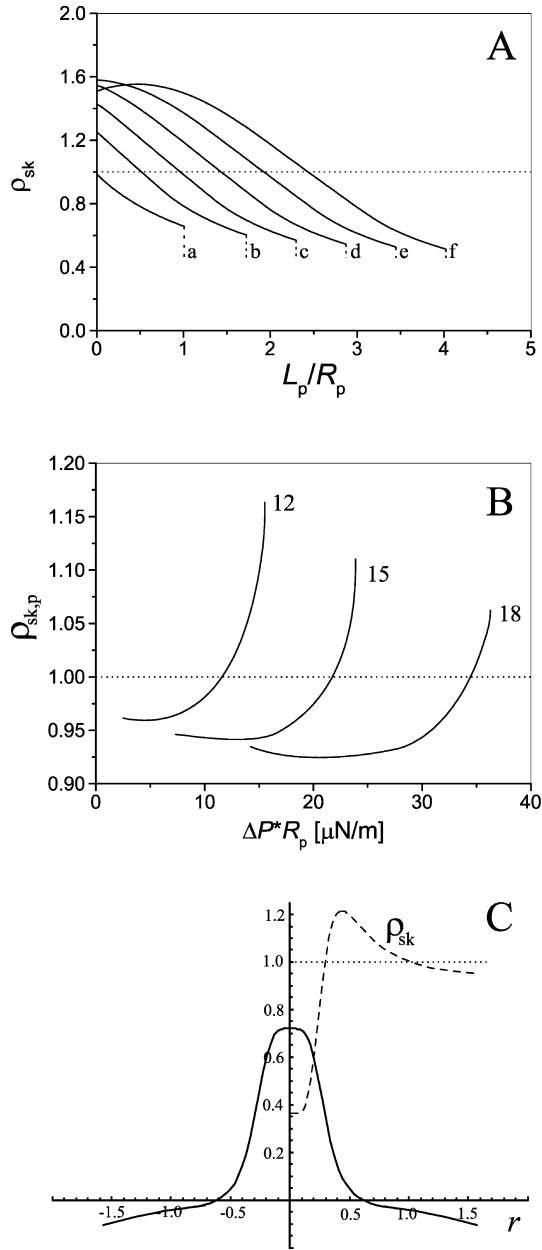


**Fig. 5A–C** Predicted distribution of the skeletal density. **A** The local density of the skeleton  $\rho_{sk}$  as a function of the distance along the cell projection for different values of  $L_p/R_p$ : The corresponding values of  $\Delta P R_p$  (in  $\mu\text{N/m}$ ) are: (a) 8.1, (b) 15.2, (c) 19.1, (d) 22.0, (e) 23.7, and (f) 23.8. Curve (f) represents  $\rho_{sk}$  at the critical aspiration pressure. (The area difference  $\Delta a_0 = 15$ , and other material constants are as in Fig. 3). **B** The skeletal density averaged over the entire aspirated projection  $\rho_{sk,p}$  as a function of the aspiration pressure for the indicated values of  $\Delta a_0$  (12, 15, 18). The other elastic properties are the same as in Fig. 3. Above the dotted line ( $\rho_{sk} = 1$ ) the skeleton is condensed, below the dotted line it is expanded. **C** The predicted distribution of skeletal density (dashed line) along a spicule contour (solid line) as a function of radial position

instructions. Filled pipettes were stored in filtered distilled water.

Chambers were made from two siliconized cover glasses separated by a plastic spacer  $\sim 1.0$  mm in

thickness. The chamber was U-shaped with the open side to allow access for measuring and reference pipettes. An inverted Nikon microscope with a video camera (Dage-MTI, Michigan City, IN, USA, CCD72S) was used in these studies. The illumination was monochromatic (436 nm). The image from the camera was superimposed with digital readings of the time, data, and pipette-aspiration pressure.

### Experimental procedure

The relationship between RBC deformability and morphology was examined by testing individual red blood cells over a range of echinocyte shapes. Two pipettes of different sizes were introduced into a chamber containing a suspension of cells (Fig. 6). A discoid cell was selected based on its ability to be sucked completely but snugly into the larger pipette. An echinocyte shape was induced by applying large suction pressures ( $> 20$  mm  $\text{H}_2\text{O}$ ) to the cell for several seconds using the smaller pipette, which it could not enter. After release, the cell appeared as an echinocyte, and its deformability was examined by aspiration into the larger pipette at a series of increasing pressures to determine the relationship between aspiration pressure  $\Delta P$  and the length of the aspirated projection  $L_p$ . Pressure increments were approximately 0.25 mm  $\text{H}_2\text{O}$ , and the maximum aspiration pressure did not exceed 3 mm  $\text{H}_2\text{O}$ . The critical point of the aspiration, that is, the largest pressure at which the cell can still be held in a stable equilibrium was noted, and the corresponding “critical” projection length was also measured.

After testing, the cell maintained its shape for several minutes, but over time ( $\sim 15$  min) the cell relaxed toward a more discocytic shape (Artmann et al. 1997). (See Fig. 7.) After shape relaxation, the same cell was tested again to determine the dependence of  $L_p$  on  $\Delta P$ . By allowing the shape to relax and then repeating the application of high pressure to re-establish the echinocyte shape, the same cell was tested repeatedly at different degrees of echinocytosis.

The surface area and volume of each RBC tested were measured by aspiration into the narrow pipette at 100 mm  $\text{H}_2\text{O}$  pressure. This pressure was large enough to unfold the membrane completely. The surface area ( $A_0$ ) and volume ( $V_0$ ) were calculated from the radius of the pipette  $R_p$ , the length of the cell projection in the pipette  $L_p$ , and the radius of the outer portion  $R_c$ :

$$A_0 = 2\pi(R_p - R_c)\sqrt{R_p^2 + R_c^2} \quad (21)$$

$$V_0 = \frac{2\pi}{3}\left[R_0^3 + \left(R_0^2 + \frac{R_p^2}{2}\right)\sqrt{R_0^2 - R_p^2} + R_p^3\right] + \pi R_p^2(L_p - R_p). \quad (22)$$



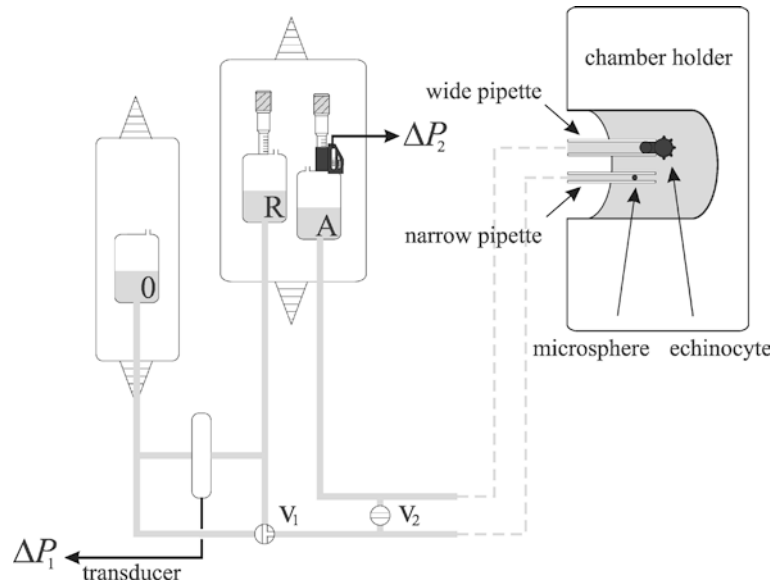


**Fig. 6** Schematic of the experimental apparatus. The *left side* of the figure illustrates the manometer system used to control aspiration pressure, and the *right side* shows a schematic view of the chamber where erythrocytes were aspirated into micropipettes. Two pipettes with different diameters were inserted into the chamber. Reservoir 0 was used to apply large aspiration pressures ( $\Delta P_1 > 10 \text{ mm H}_2\text{O}$ ) to cause cell crenation (or measure cell area and volume) via the smaller pipette ( $R_p \sim 0.7 \mu\text{m}$ ). These pressures were monitored using the pressure transducer. Reservoir A was used to apply small pressures ( $\Delta P_2 < 3.0 \text{ mm H}_2\text{O}$ ) via the larger pipette ( $R_p \sim 1.7 \mu\text{m}$ ) to measure cell deformability. These pressures were measured using a digital micrometer with 0.01 mm resolution. Reservoir R provided a zero pressure reference. During cell crenation, the stopcock  $V_1$  was turned so that R was connected to the transducer and 0 was connected to the small pipette. (The transducer reported the pressure exerted by 0 relative to R.) During deformability measurements  $V_1$  was turned so that R was connected to the pipette. In this case the motion of a small particle in the lumen of the pipette was observed to monitor zero pressure. If the particle motion indicated flow in the small pipette, the height of the plate holding reservoirs A and R was adjusted to re-establish zero pressure in the reference pipette. In this way the measured displacement of A relative to R always gave an accurate measure of the suction applied to the cells. The stopcock  $V_2$  was normally closed, but could be opened to equilibrate the pressures between A and R

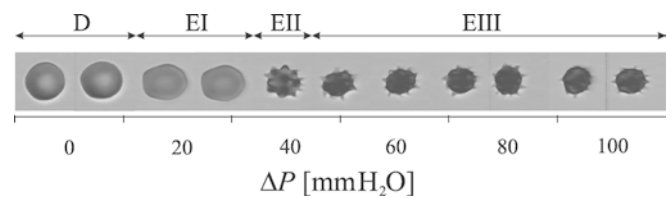


**Fig. 7** Echinocytosis was induced by micropipette aspiration. The degree of crenation increased with increasing aspiration pressure  $\Delta P$ . Cell morphology is indicated according to the red cell shape classification of Bessis (1973): D is a discocyte, EI is a flat erythrocyte with irregular contour, EII is flat erythrocyte with a few spicules, and EIII is an ovoid or spherical cell with 30–50 spicules

In addition to the relationship between projection length and pressure, the change in morphology of the unaspirated portion of the cell was also observed. The spicules on the cell body were observed to disappear individually in such a way that the height of a disappearing spicule decreased rapidly. Interestingly, the size and shape of the remaining spicules did not vary significantly as the projection length increased.

Measurements made on discoid cells and lower stages of echinocyte are not shown. The more disk-like shape of these cells was not well approximated by the model of a sphero-echinocyte used in the theoretical calculations. Generally, the curves for discoid cells were steeper than the curves for echinocytes, meaning that discoid cells were more easily aspirated into the pipette. Furthermore, the critical pressure was lower and the critical cell projection length was larger for discocytes than for echinocytes.

## Experimental results

The relationship between projection length and aspiration pressure is shown in Fig. 8 for a single cell aspirated into a pipette at different degrees of echinocytosis. This is one of five cells tested, all of which showed similar behavior. It is clear from the results shown in Fig. 8 that the pressures required to aspirate the cell depended on the degree of echinocytosis. This is manifested by both a change in the slope of the curves and a shift of the data toward higher  $\Delta P R_p$ . Furthermore, the critical pressure increased with the degree of echinocytosis. Note that the dependence of aspiration length on pressure correlated with the degree of crenation regardless of how many times the cell was previously aspirated into the pipette.

## Discussion

The RBC membrane is a composite of lipid bilayer and an underlying protein skeleton, and the mechanical properties of this composite are the principal

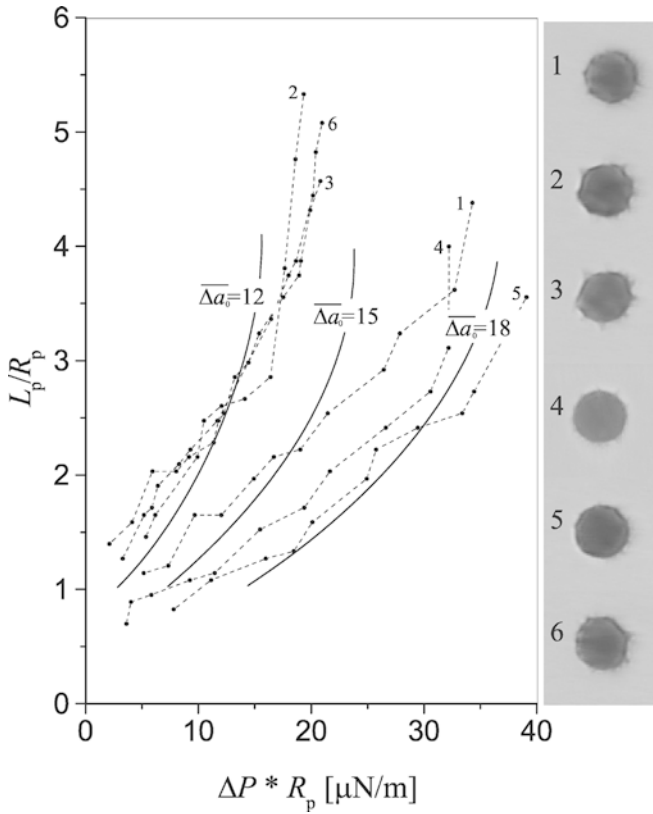


**Fig. 8** The ratio between the equilibrium projection length and the pipette radius as a function of the aspiration pressure scaled by the pipette radius. Measured data are represented by points connected by dashed lines. Deformation of a single erythrocyte was measured for several different initial shapes induced by high aspiration pressure (1–6). Shape numbers correspond to the order of successive applications of high pressure separated by periods of shape relaxation. Note that shapes 1, 4, and 5 are spherical with many small spicules, while shapes 2, 3, and 6 are less spherical and the spicules are larger. According to Fig. 7, shapes 1, 4, and 5 correspond to the most severe form (EIII) stage of an echinocyte. Each *dashed curve* ends at its critical point, which was carefully measured as described in the text. *Solid curves* show the theoretical predictions for projection length as a function of pressure for the indicated values of  $\Delta a_0$ . The cellular volume and surface area used in the calculations were those measured using the narrow pipette:  $V_0 = 109 \mu\text{m}^3$ ,  $A_0 = 140 \mu\text{m}^2$ . The remaining membrane elastic properties were set to be  $\mu = 6 \mu\text{N/m}$ ,  $K = 2\mu$ ,  $k_c = 2 \cdot 10^{-19} \text{ J}$ ,  $k_r = 4k_c$ .

determinants of cell morphology and the response of the cell to external forces (Mohandas and Chasis 1993; Mohandas and Evans 1994). Constitutive laws for the behavior of the membrane composite have been developed, and the characteristic coefficients have been estimated, primarily from observations of partial aspiration of cells into micropipettes. Opportunities to test the predictive power of constitutive models are rare, because the experimental options for modifying cell shape under controlled conditions are limited. This is particularly true for cases in which the membrane bilayer and the membrane skeleton both play significant roles in determining the cellular response. Thus, analysis and measurement of the aspiration of red cell echinocytes into micropipettes represents an unusual opportunity to

study contributions of both the skeletal and lipid bilayer elasticity to RBC deformability. We demonstrate that the relationship between cell deformability and the degree of crenation can be attributed to the modification of the bilayer equilibrium area difference  $\Delta a_0$ . The assumptions underlying the analysis, the significance of the experiments, and the relationship of the present results to published studies are discussed in the following paragraphs.

It is widely recognized that the elastic behavior of the cell membrane includes contributions from the local and nonlocal bending of the bilayer as well as the shear and area expansivity of the membrane skeleton, subject to the constraint of constant membrane surface area. Most published studies of red cell deformation tend to focus on cases in which an individual aspect of cell elasticity predominates, and other contributions can be neglected. An important exception to this is the transformation of cell shape from discocyte to echinocyte. Several studies have recognized that both skeleton shear elasticity and bilayer bending elasticity must be considered to properly account for stable spicule formation. Early studies of this problem treated membrane skeleton as incompressible (Waugh 1996; Igljč 1997) but a more recent report extended the treatment to include the elastic compression and dilation of the skeleton (Mukhopadhyay et al. 2002). In the absence of time-dependent effects, these contributions to the membrane elastic energy constitute a minimal but complete model for the analysis of RBC deformability.

In the present work it is assumed that the elastic coefficients are independent of material deformation and time. Accordingly, all deformations of the skeleton are calculated relative to the same initial discocyte state. The assumption of time independence limits the applicability of the model to deformations of relatively short duration. In addition, a relatively simple relationship is used for the skeleton elasticity (see Eqs. 8 and 9). Other more complicated formulations have been proposed (Mohandas and Evans 1994; Discher et al. 1998; Lim et al. 2002), but for small to moderate deformations, the simpler form used here results in similar predictions for cell behavior and at substantially less computational effort (Waugh et al. in preparation).

The parametric approximation used to describe the cell shape captures the essential features of the deformation and enables the computations to be done with a modest computational effort. We note that the predicted relationship between projection length ( $L_p/R_p$ ) and applied pressure ( $\Delta P * R_p$ ) obtained with the present model is substantially different from the linear length–pressure relationship that is characteristic of discocyte aspiration models (Evans and La Celle 1975; Mohandas and Evans 1994). Results of the analysis (Fig. 3) clearly show that echinocyte deformability is affected by changes in  $\Delta a_0$ . The shift in the predicted curve toward the higher pressure as  $\Delta a_0$  is increased is a direct consequence of the nonlocal bending contribution to the thermodynamic potential. By minimizing the thermodynamic

potential  $G$  according to Eq. (20), the product  $\Delta P^* R_p$  can be expressed as two terms, one that is a function of the ratio  $L_p/R_p$ , and another that is linear in  $\overline{\Delta a_0}$ . The later term is equal to  $3 * \overline{\Delta a_0}$  ( $\mu\text{N}/\text{m}$ ) (for the values of elastic properties used in Fig. 3). Hence, if  $\overline{\Delta a_0}$  is increased by one, the length–pressure curve shifts by  $3 \mu\text{N}/\text{m}$  toward higher pressure.

In addition to the lateral shift in the predicted curve (the primary consequence of changing) it is evident from Fig. 3 that the predicted relationship is nonlinear and that the slope of the curve also depends on  $\overline{\Delta a_0}$ .

This effect can be understood by considering the way that  $\overline{\Delta a_0}$  affects the skeleton density distribution in the deformed echinocyte membrane. The recognition that skeleton density does change during deformation is an important and relatively recent development in our understanding of red cell membrane mechanics. Experimentally it was demonstrated that the deformation of the membrane during pipette aspiration causes lateral redistribution of the membrane skeleton (Discher et al. 1994; Artmann et al. 1998), such that in regions where the shear deformation is highest, density increased, and where shear deformation is low, the density decreased. This effect can be understood on the basis of energy minimization in response to axisymmetric deformation. As the membrane is pulled into the pipette each section of the membrane must decrease its circumference. In this case it is energetically more favorable for the system to decrease the energy of shear deformation by increasing its local density, thus trading an increase in dilational energy for a larger decrease in shear energy. (At increasing density, the extension ratio along the axis  $\lambda_m$  becomes smaller, decreasing the difference between the extension ratios  $\lambda_m$  and  $\lambda_\phi$ .) Because the skeleton is attached to the lipid bilayer there is a constraint on the total skeleton surface area, requiring that when there is condensation of the skeleton in regions where shear deformation is high, dilation must occur in regions where shear deformation is low. This reasoning applies to the shape transformation during both pipette aspiration and spicule formation.

During the aspiration of an echinocyte into a pipette, there are two competitive skeleton deformation effects: one caused by spicule formation and the other caused by membrane aspiration into the pipette. The skeleton is initially “caught” in the higher deformation regions of the spicules. At small aspiration pressures it is less favorable for the skeleton to be moved from spicules into the aspirated part of the membrane, causing the skeleton to be relatively compressed in the region outside the pipette and expanded in the aspirated portion. This results in an extra resistance to aspiration of the cell into the pipette. However, when the deformation in the aspirated portion is larger, the balance shifts toward higher density in the aspirated portion, leading to easier aspiration of the cell as the skeleton shifts from the spicules to the aspirated portion. This effect is evident in Fig. 5B, where it is clear that increasing  $\overline{\Delta a_0}$  increases the pressure at which the skeletal density inside the

pipette begins to increase. This prediction is confirmed experimentally (Fig. 8).

Testing of the analytical predictions required an experimental procedure in which a change in cell morphology is driven by an imposed change in the leaflet area difference, while all other mechanical parameters remain constant. A convenient method for modifying cell shape has been described by Artmann et al. (1997), who demonstrated that RBC can be crenated mechanically by high-pressure aspiration into a narrow pipette. Artmann et al. (1997) showed that the discocyte–echinocyte shape transformation induced by this approach is due to a transmembrane phospholipid translocation that leads to an equilibrium area difference between leaflets of the bilayer, while alteration in the skeleton is not a primary factor for inducing shape change. An important condition for the applicability of the analysis to the experiments is that the condition of the cell should be stable over the time course of an individual measurement. Mechanically induced echinocytes relax back to a biconcave shape, but the time required to test cell deformability ( $\sim 1$  min) was short compared to the characteristic time for shape relaxation ( $\sim 15$  min; this study; Artman et al. 1997). Thus, the resting shape of the cell was sufficiently stable during our tests of cell deformability. Because cell deformability was also determined by micropipette aspiration, precautions were taken to ensure that additional induction of shape change was not induced by the deformability test. Cells were selected that fit easily but snugly into the larger pipette lumen used for testing deformability. Thus, pressures applied in the deformability tests ( $< 3$  mm H<sub>2</sub>O) were substantially less than pressures applied to cause shape change ( $> 10$  mm H<sub>2</sub>O), and were unlikely to induce further crenation of the cell.

Measurements of the aspiration pressure required to pull echinocytes of different degrees of severity into a micropipette confirm the prediction of the analysis, and support the conclusion that the bilayer leaflet area difference accounts for the increased resistance to deformation. There is general consensus that changes in the interleaflet area difference are what drive echinocyte formation (Sheetz and Singer 1974; Waugh 1996; Iglıć 1997; Mukhopadhyay et al. 2002). The increased resistance to deformation measured in the present study is characterized by both a change in the slope of the curve and a shift toward higher values of  $\Delta P^* R_p$ . Significantly, the magnitude of these changes correlates with the severity of crenation, and by implication, with the magnitude of  $\overline{\Delta a_0}$  in the membrane. Past investigators have observed increased cell rigidity for echinocytes (Chabanel et al. 1987; Bessis et al. 1973). Chabanel et al. (1987) induced echinocytes using salicylate, and studied cell deformability by the pipette test. They interpreted the increased slope of the length–pressure curves as a change in membrane shear modulus (based on the work of Evans and La Celle 1975), but they did not perform a thorough analysis of the possible contributions of membrane bending and could not account for the

accompanying shift in the curves to higher pressures. Our model calculations show that this behavior can in general be ascribed simply to the modification of  $\Delta a_0$ , and therefore, it appears likely that their results reflect a change in  $\Delta a_0$  caused by salicylate. Note that the theoretical curves in Fig. 8 differ only in the value of  $\Delta a_0$ , while all the other elastic parameters are fixed. While one might argue that the approximate geometry we have used in the analysis could lead to small quantitative errors in the values of  $\Delta a_0$  that correlate with our experimental results, the similarity of the model geometry to that of the real cells indicates that our values should be reliable estimates of the true values.

## Conclusions

In this report we analyzed the contribution of the bilayer elastic properties to RBC deformability examined by whole cell micropipette aspiration. It was hypothesized that the modification of the cell shape to an echinocyte and the corresponding changes in cell deformability can be understood in terms of a single comprehensive description of the elastic behavior of the cell membrane. The corresponding model was developed and its predictions were compared to experiment. Our findings support the conclusions of prior studies that a change in the bilayer leaflet area difference drives the change in cell shape to an echinocyte. We extend those conclusions to show that the decreased deformability of echinocytes can be ascribed to the same mechanism, without invoking changes in other elastic coefficients that characterize the cell membrane.

## Appendix A. Elimination of cell shape parameters $r_b$ , $L_0$ , and $R_c$

The shape of the echinocyte is defined parametrically by six parameters ( $L_0$ ,  $r_b$ ,  $R_c$ ,  $N_b$ ,  $r_c$ , and  $L_p$ ). Three of them can be derived from the geometrical conditions: the cell surface area is constant, the cell volume is constant, and spicules connect smoothly to the spherical cell body with a radius  $R_c$ . The remaining three parameters are determined with the minimization of thermodynamic potential (Eq. 16).

It can be shown that it is more convenient to derive  $L_0$ ,  $r_b$ , and  $R_c$  from geometrical conditions that are expressed by the following equations:

$$A_0 = A_p + A_s + N_b A_b, \quad (23)$$

$$V_0 = V_p + V_s + N_b V_b, \quad (24)$$

$$\left. \frac{dz_b}{dr} \right|_{r_b} = -\frac{r_b}{\sqrt{R_c^2 - r_b^2}}. \quad (25)$$

In Eq. (23),  $A_p$  is the surface area of the aspirated membrane projection,  $A_s$  is the surface area of the

spherical portion of the cell body (excluding the bases of all the spicules and the pipette entrance), and  $A_b$  is the surface area of each spicule:

$$A_p = 2\pi R_p L_p, \quad (26)$$

$$A_s = 4\pi R_c^2 - N_b \cdot 2\pi R_c \left( R_c - \sqrt{R_c^2 - r_b^2} \right) - 2\pi R_c \left( R_c - \sqrt{R_c^2 - R_p^2} \right), \quad (27)$$

$$A_b = 2\pi \int_0^{r_b} r \cdot \sqrt{1 + \left( \frac{dz_b}{dr} \right)^2} \cdot dr. \quad (28)$$

Similarly, in Eq. (24),  $V_p$  is the volume of the cell portion aspirated into the pipette,  $V_s$  is the volume of the spherical cell body (adjusted for the volume of the portion that is in pipette entrance),  $V_b$  is the volume of the spicule (adjusted for an overlapping volume between the spicule and the spherical cell body):

$$V_p = \pi R_p^2 \left( L_p - \frac{R_p}{3} \right), \quad (29)$$

$$V_s = \frac{4}{3} \pi R_c^3 - \pi h_1^2 (R_c - h_1/3), \quad (30)$$

$$V_b = \frac{1}{2} r_c^2 \pi L \left[ \pi - 2 \arctan \left( 1 - \sqrt{2} \frac{r_b}{r_c} \right) - 2 \arctan \left( 1 + \sqrt{2} \frac{r_b}{r_c} \right) \right] - \pi r_b^2 z_b(r_b) - \pi h_2^2 (R_c - h_2/3), \quad (31)$$

where  $h_1$  and  $h_2$  are:

$$h_1 = R_c - \sqrt{R_c^2 - R_p^2}, \quad (32)$$

$$h_2 = R_c - \sqrt{R_c^2 - r_b^2}. \quad (33)$$

The third constraint, related to the smooth joining of the spicule to the spherical cell body (Eq. 25), leads to an expression for the spherical cell radius  $R_c$ :

$$R_c = r_b \sqrt{1 + \frac{r_c^8 L^4}{16[r_b + z_b(r_b)]^6}}. \quad (34)$$

The variable  $L$  is a difference between the maximal and minimal value of the contour function (Eq. 10) and it is related to the spicule height  $L_0$ :

$$L = L_0 + z_b(r_b) - \sqrt{R_c^2 - r_b^2} + R_c. \quad (35)$$

In contrast to the equation for  $R_c$  (Eq. 34), Eqs. (23) and (24) cannot be solved explicitly for the parameters  $L_0$  and  $r_b$ . Therefore, the equations were solved numerically by a simple bisection method. For specified values of  $N_b$ ,  $r_c$ , and  $L_p$ , the parameter  $r_b$  was modified to find a root of the ‘‘area equation’’ (Eq. 23). For each

value of  $r_b$ , a value for  $L_o$  was calculated from the “volume equation” (Eq. 24). Then  $R_c$  could be expressed explicitly with Eq. (34).

## Appendix B. Bending energy of the bilayer

Contributions to the local bending energy  $W_b$  in Eq. (12) are calculated according to Eq. (7). For the portion of the cell in the pipette, and for the spherical cell body, these resolve to:

$$W_b^p = 4\pi k_c \left(1 - \frac{L_p - R_p}{4R_p}\right), \quad (36)$$

$$W_b^s = 2k_c \frac{A_s}{R_c^2}. \quad (37)$$

For the spicules,  $W_b^b$  is obtained by numerical integration of Eq. (7) along the spicule surface. The principal curvatures are defined as follows:

$$c_p = \frac{\sin \theta}{m} \quad \text{and} \quad c_m = \frac{d}{ds}, \quad (38)$$

where  $\theta$  is the angle between the local normal and the symmetry axis. The shape of the cell contour  $z(r)$  is known, and therefore it is convenient to rewrite Eqs. (38) as follows:

$$c_p = \frac{1}{r \cdot P} \cdot \frac{d}{dr} \quad \text{and} \quad c_m = \frac{1}{P^2 dz/dr} \cdot \frac{d}{dr}, \quad (39)$$

$$P = \frac{ds}{dr} = \sqrt{1 + \left(\frac{dz}{dr}\right)^2}. \quad (40)$$

Evaluating the derivatives leads to the following expressions for the principal curvatures  $c_m$  and  $c_p$ :

$$c_m = \frac{12r^2}{r_c^2 L^2} \left[1 - \frac{5}{3} \left(\frac{r}{r_c}\right)^4\right] \cdot \left(\frac{z_b(r)}{P_b}\right)^3$$

and

$$c_p = \frac{4r^2 z_b(r)^2}{r_c^4 L P_b} \quad (41)$$

( $P_b$  stands for  $P$  (Eq. 40) calculated for the spicule contour).

Calculation of the nonlocal bending energy requires evaluation of  $\Delta a$  (Eq. 13). For the pipette projection and the spherical portion of the cell body, the relevant expressions are:

$$\Delta a^p = \frac{L_p + R_p}{4R_0}, \quad (42)$$

$$\Delta a^s = \frac{R_c}{4\pi R_0} A_s. \quad (43)$$

For the spicules,  $\Delta a^b$  was calculated by numerical integration of Eq. (4) using the expressions for the

principal curvatures given in Eq. (41). An additional term,  $\Delta a^T$ , arises from a leaflet area difference of the junction between the spherical cell body and the cell projection in the pipette. The leaflet area difference of that small region of high curvature was estimated by treating the junction as a torus that matches slopes with the cylindrical projection in the pipette and the spherical outer section. Thus, the larger radius of the torus is equal to  $R_p$ . The expression for  $\Delta a^T$  was obtained by taking the limit as the smaller radius approaches zero:

$$\Delta a^T = -\frac{R_p}{4R_0} \left(\frac{\pi}{2} - \arcsin \frac{R_p}{R_c}\right), \quad (44)$$

## Appendix C. Elastic energy of the skeleton

Deformation of the membrane skeleton is characterized by the mapping of a small skeleton portion from its resting location to the deformed one, where the mapping function is obtained by minimizing the deformation energy of the skeleton ( $W_{sk}$ ). As described in the Theory section, the resting shape of the membrane is assumed to be discoid and the shape of the deformed membrane is constructed from different geometric units: a spherical cell body, spicules, and a cell projection (Fig. 9). Both the resting and deformed shapes of the membrane skeleton are specified by contour functions  $r_0(s_0)$  and  $r(s)$ . These are shown in Table 1 (cell projection formation) and in Table 2 (spicule formation). Axisymmetric mapping of a small portion of the skeleton from its resting location at  $(s_0, r_0)$  to the deformed one at  $(s, r)$ , can be defined by a single parametric mapping function:

$$s_0 = s_0(s). \quad (45)$$

Deformation of that small portion of the skeleton is described by material extension ratios defined by Eq. (14):

$$\lambda_1 = \frac{r(s)}{r_0(s_0)} \quad \text{and} \quad \lambda_2 = \frac{1}{s'_0}, \quad (46)$$

where  $s'_0 = ds_0/ds$ . The mapping function  $s_0(s)$  is obtained by the minimization of the elastic energy of the skeleton  $W_{sk}$  (Eqs. 8 and 9), which can be expressed as a function of  $s_0(s)$  and its derivative only.  $W_{sk}$  is obtained by integration over deformed membrane surface:

$$W_{sk}(s_0, s'_0) = 2\pi \int \ell(s, s_0, s'_0) \cdot ds, \quad (47)$$

where  $\ell(s, s_0, s'_0)$  takes the form:

$$\ell(s, s_0, s'_0) = \left\{ \frac{\mu}{2} \cdot \left[ \frac{r(s)}{r_0(s_0)} - \frac{1}{s'_0} \right]^2 + \frac{K}{2} \cdot \left[ \frac{r(s)}{r_0(s_0)} + \frac{1}{s'_0} - 2 \right]^2 \right\} r_0(s_0) s'_0. \quad (48)$$

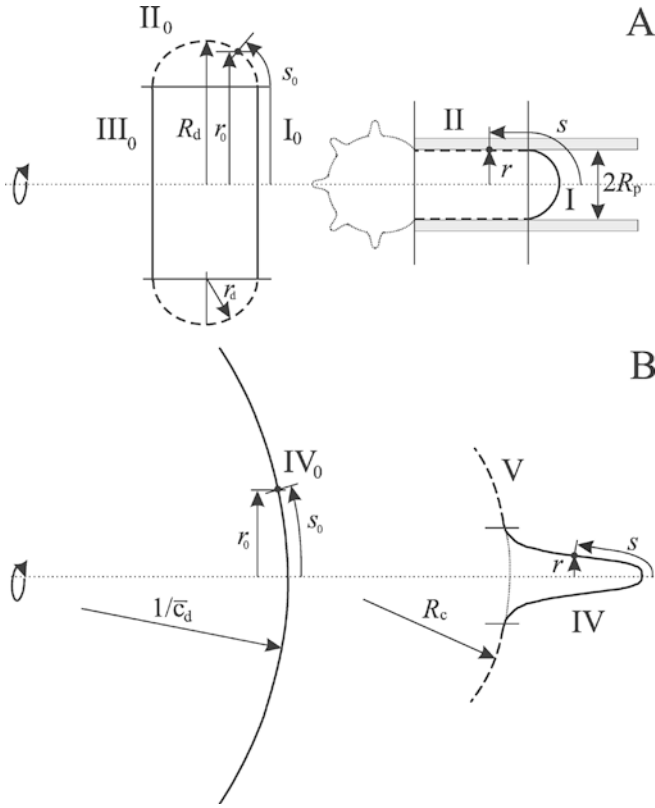


**Fig. 9** Membrane regions of the cell contour for membrane deformation due to pipette aspiration (a) and spicule formation (b). The different regions are distinguished by dashed and solid lines and designated by  $I_0, I$ , etc. The position of the material point is defined by radial and meridional coordinates,  $r_0$  and  $s_0$  for the resting contour (left side of the figure),  $r$  and  $s$  for the deformed contour (right side of the figure). Axes of symmetry are indicated by dotted lines

**Table 1** Parametric description of the cell projection contour and the corresponding resting membrane contour; see Fig. 9a

Map. unit	$r_0(s_0)$	$r(s)$
$I_0 \rightarrow I$	$s_0$	$R_p \sin \frac{s}{R_p}$
$I_0 \rightarrow II$	$s_0$	$R_p$
$II_0 \rightarrow I$	$R_d - r_d(1 - \sin \frac{s_0 - R_d}{r_d})$	$R_p \sin \frac{s}{R_p}$
$II_0 \rightarrow II$	$R_d - r_d(1 - \sin \frac{s_0 - R_d}{r_d})$	$R_p$
$III_0 \rightarrow II$	$2(R_d - r_d) + \pi r_d - s_0$	$R_p$

**Table 2** Parametric description of the spicule contour and the corresponding resting membrane contour; see Fig. 9b

Map. unit	$r_0(s_0)$	$r(s)$
$IV_0 \rightarrow IV$	$\frac{\sin(\bar{c}_d s_0)}{\bar{c}_d} *$	**
$IV_0 \rightarrow V$	$\frac{\sin(\bar{c}_d s_0)}{\bar{c}_d}$	$R_C \cdot \sin \frac{s - s_b}{R_C} ***$

\*Average curvature of the resting discoid cell shape  $\bar{c}_d = \frac{\pi}{A_0} [\pi R_d + (4 - \pi) r_d]$ .

\*\* $r(s)$  for the spicule contour is obtained numerically by the use of Eq. (10).

\*\*\* $s_b$  is meridian distance from the top of the spicule to its base, and it is calculated numerically.

In order to minimize  $W_{sk}$  (Eq. 47),  $s_0(s)$  is derived by solving the Euler–Lagrange equation

$$\frac{\partial \ell(s, s_0, s'_0)}{\partial s_0} - \frac{d}{ds} \frac{\partial \ell(s, s_0, s'_0)}{\partial s'_0} = 0. \quad (49)$$

Separate numerical solutions are obtained for the aspirated projection and for the outer cell portion. To solve the Euler–Lagrange equation, the values of the mapping function and its derivative at the initial point are required. They must satisfy boundary conditions. The central point of the resting skeleton must map onto the apex of the deformed shape (either the tip of the spicule located on the axis of symmetry or the tip of the cell projection). The total surface area of the skeleton must not change during its deformation, and the lateral tension of the aspirated part must match the lateral tension of the outer part of the cell. Note that the relative proportion of the resting skeleton that is either aspirated into the pipette or deformed into the outer sphero-echinocytic portion is not fixed. In our approach the relative proportion of resting skeleton in the pipette or on the cell body was varied to obtain the minimal skeleton deformation energy, and thus to assure matching of the lateral tensions.

## References

- Artmann GM, Kelemen C, Porst D, Büldt G, Chien S (1998) Temperature transitions of protein properties in human red blood cells. *Biophys J* 75:3179–3183
- Artmann GM, Sung KLP, Horn T, Whittemore D, Norwich G, Shu C (1997) Micropipette aspiration of human erythrocytes induces echinocytes via membrane phospholipid translocation. *Biophys J* 72:1434–1441
- Bazzoni G, Rasia M (1998) Effects of an amphipathic drug on the rheological properties of the cell membrane. *Blood Cell Mol Dis* 24:552–559
- Bessis M (1973) Red cell shapes. An illustrated classification and its rationale. In: Bessis M, Weed RI, Leblond PF (eds) *Red cell shape—physiology, pathology, ultrastructure*. Springer, Berlin Heidelberg New York, pp 1–24
- Boey SK, Boal DH, Discher DE (1998) Simulations of the erythrocyte cytoskeleton at large deformation. I. Microscopic models. *Biophys J* 75:1573–1583
- Božič B, Svetina S, Žekš B, Waugh RE (1992) Role of membrane structure in tether formation from bilayer vesicles. *Biophys J* 61:963–973
- Chabanel A, Reinhart W, Chien S (1987) Increased resistance to membrane deformation of shape-transformed human red blood cells. *Blood* 69:739–743
- Deuticke B (1968) Transformation and restoration of biconcave shape of human erythrocyte induced by amphiphilic agents and changes of ionic environment. *Biochim Biophys Acta* 163:494–500
- Discher DE, Boal DH, Boey SK (1998) Simulations of the erythrocyte cytoskeleton at large deformation. II. Micropipette aspiration. *Biophys J* 75:1584–1597
- Discher DE, Mohandas N, Evans EA (1994) Molecular maps of red-cell deformation: hidden elasticity and in situ connectivity. *Science* 266:1032–1035
- Eggleton CD, Popel AS (1998) Large deformation of red blood cell ghosts in a simple shear flow. *Phys Fluids* 10:1834–1845
- Evans EA (1973) New membrane concept applied to the analysis of fluid shear- and micropipette-deformed red blood cells. *Biophys J* 13:941–954

- Evans EA, La Celle PL (1975) Intrinsic material properties of erythrocyte membrane indicated by mechanical analysis of deformation. *Blood* 45:29–43
- Evans EA, Skalak R (1980) *Mechanics and thermodynamics of biomembranes*. CRC Press, Boca Raton, FL
- Helfrich W (1973) Elastic properties of lipid bilayers—theory and possible experiments. *Z Naturforsch C* 28:693–703
- Hénon S, Lenormand G, Richert A, Gallet F (1999) A new determination of the shear modulus of the human erythrocyte membrane using optical tweezers. *Biophys J* 76:1145–1151
- Hochmuth RM, Waugh RE (1987) Erythrocyte membrane elasticity and viscosity. *Ann Rev Physiol* 49:209–219
- Hwang WC, Waugh RE (1997) Energy of dissociation of lipid bilayer from the membrane skeleton of red blood cells. *Biophys J* 72:2669–2678
- Iglić A (1997) A possible mechanism determining the stability of spiculated red blood cells. *J Biomech* 30:35–40
- Lenormand G, Hénon S, Richert A, Siméon J, Gallet F (2001) Direct measurement of the area expansion and shear moduli of the human red blood cell membrane skeleton. *Biophys J* 81:43–56
- Li A, Seipelt H, Müller C, Shi YD, Artmann GM (1999) Effects of salicylic acid derivatives on red blood cell membranes. *Pharmacol Toxicol* 85:206–211
- Lim GHW, Wortis M, Mukhopadhyay R (2002) Stomatocyte–discocyte–echinocyte sequence of the human red blood cell: evidence for the bilayer-couple hypothesis from membrane mechanics. *Proc Natl Acad Sci USA* 99:16766–16769
- Meiselman HJ (1981) Morphological determinants of red cell deformability. *Scand J Clin Lab Inv* 41, Suppl 156:27–34
- Mohandas N, Chasis JA (1993) Red blood cell deformability, membrane material properties and shape: regulation by transmembrane, skeletal and cytosolic proteins and lipids. *Semin Hematol* 30:171–192
- Mohandas N, Evans EA (1994) Mechanical properties of the red cell membrane in relation to molecular structure and genetic defects. *Ann Rev Biophys Biomol Struct* 23:787–818
- Mukhopadhyay R, Lim G, Wortis M (2002) Echinocyte shapes: Bending, stretching, and shear determine bump shape and spacing. *Biophys J* 82:1756–1772
- Reinhart WH, Chien S (1986) Red cell rheology in stomatocyte–echinocyte transformation: roles of cell geometry and cell shape. *Blood* 67:1110–1118
- Sheetz MP, Singer SJ (1974) Biological membranes as bilayer couples—molecular mechanism of drug erythrocyte interactions. *Proc Natl Acad Sci USA* 71:4457–4461
- Svetina S, Brumen M, Žekš B (1985) Lipid bilayer elasticity and the bilayer couple interpretation of the red cell shape transformations and lysis. *Studia Biophysica* 110:177–184
- Svoboda K, Schmidt CF, Branton D, Block SM (1992) Conformation and elasticity of the isolated red blood cell membrane skeleton. *Biophys J* 63:784–793
- Waugh RE (1996) Elastic energy of curvature-driven bump formation on red blood cell membrane. *Biophys J* 70:1027–1035